Monolithically integrated InP optical 90° hybrid

H. O. Çirkinoglu, R. Santos, K. Williams, and X. Leijtens

Eindhoven University of Technology, 5612 AZ, Eindhoven, The Netherlands

An optical 90°hybrid is used for demodulating the information encoded in the phase and amplitude of an incoming optical signal by interfering it either with a local oscillator or with itself. Such 90° hybrids are essential for retrieving the amplitude of both orthogonal quadratures of the received signal in applications such as coherent communications, or continuous-variable quantum key distribution. In this work, we report on the design and the results from a monolithically integrated optical 90° hybrid, based on a 4×4 multi-mode interference coupler fabricated in the generic InP platform of Smart Photonics. We investigated the performance of the hybrid in terms of its common-mode rejection ratio, and phase mismatch across the full C-band.

Introduction

Optical communication systems where information is encoded in both quadratures of light offer improved spectral efficiency compared to conventional methods relying on intensity modulation/direct detection [1,2]. At the receiver side of such systems, the amplitude and phase of the incoming signal is required to be converted into the electrical domain with high sensitivity [3]. The key components that enable this functionality include high-performance optical components such as narrow linewidth lasers, balanced photodetectors, and optical 90 hybrids [4].

A variety of methods and technologies have been used to develop optical 90° hybrids including free space optics [5], $LiNbO_3$ material platforms [6,7], as well as monolithically integrated Si based [8, 9, 10] and InP based [11, 12] photonic integrated circuits (PICs). In this work, we report on the characterization results from an InP based monolithically integrated multi-mode interference (MMI) coupler-based 90° hybrid, fabricated in a generic multi-project-wafer (MPW) run of Smart Photonics.

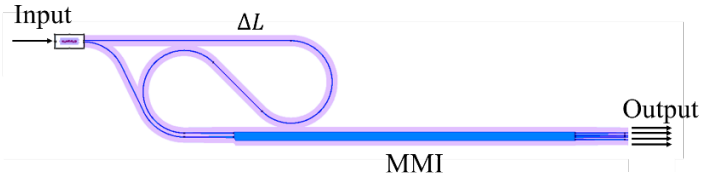

Figure 1 – The layout of the 90° hybrid test structure

90° Hybrid and the test structure

The fabricated 90° hybrid is based on a 4×4 MMI structure, where only two of the MMI inputs are used for either the signal or the local oscillator. The MMI input-output interfaces are tapered to match the width of the integrated waveguides, which carry the signal across and in/out of the chip. The characterization of the MMI is performed using an interference-based test structure as shown in Figure 1, where a single input signal is first split in two with a 1×2 MMI splitter. One of the two signals is then transferred

through an additional delay-line with a known length. The two signals are then used as the two inputs of the 90° hybrid, resulting in the signal amplitudes at the output arms as,

$$\begin{bmatrix} E_1 \\ E_2 \\ E_3 \\ E_4 \end{bmatrix} = \frac{1}{C} \begin{bmatrix} e^{j\pi} & e^{j\frac{3\pi}{4}} \\ e^{j\frac{-\pi}{4}} & e^{j\pi} \\ e^{j\frac{3\pi}{4}} & e^{j\pi} \\ e^{j\pi} & e^{j\frac{-\pi}{4}} \end{bmatrix} \begin{bmatrix} E_0 \\ E_0 e^{-i\Delta\theta} \end{bmatrix} \quad (1)$$

where E_0 is the input signal and $e^{-i\Delta\theta}$ is the phase acquired by the signal travelling through the delay line. E_{i} denotes the signal at the i^{th} output. The MMI transfer matrix above assumes the ideal operation where each s-parameter shares the same complex amplitude factor of $\frac{1}{C}$, together with their corresponding phase relations. For the fabricated devices, each parameter of the transfer matrix s_{ij} have amplitude and phase deviation, deteriorating the performance of the hybrid. In the following section, extraction and analysis of such parameters from the measurement data is explained and presented.

Measurements and analysis

The measurements are performed by using a monochromatic tunable laser source as the input signal. The optical input/output coupling is realized through lensed fibers, and angled/tapered waveguides to ensure good coupling and minimize reflections. Before the input fiber, the light is transmitted through a polarizer which, together with polarization maintaining fibers, ensures linearly polarized input light. The output light from each output port of the test structure is measured and recorded while the wavelength of the input laser is swept between 1520nm-1570 nm.

Considering the transfer matrix of the MMI in equation (1), the measured current through the photodetectors at each output port is given by,

$$I_i = R\,|E_0|^2\,|s_{i1} + s_{i2}\,e^{-i(\varphi_i+\Delta\theta)}|^2, \quad (2)$$

where $\varphi_i = \arg\{s_{i1}\} - \arg\{s_{i2}\}$. The constant R includes the optical insertion and transmission loss, together with the photodetector responsivity, and assumed to be equal for each channel. For the sake of simplicity, the imbalance of the 1×2 splitter, and the additional transmission loss through the delay line is assumed to be zero. The additional acquired phase due to the length difference is,

$$\Delta\theta = \frac{2\pi}{\lambda}\Delta L\, N_e(\lambda), \quad (3)$$

Where ΔL is the geometric length of the delay line, which is designed to be 1038 μm. N_e is the wavelength dependent effective refractive index, and λ is the wavelength.

Figure 3(a) shows the measured power for an input power of 1mW across a 2nm wavelength range, normalized for 3dB loss per fiber-chip coupling. As the wavelength of the input laser shifts, the acquired phase through the delay line ($\Delta\theta$) changes, resulting in the output power being a sinusoidal function of the wavelength. Through a non-linear least squares fit method, the parameters s_{ij} , φ_i, and $\Delta\theta$ can be estimated. Based on the mean and the standard deviation of the measurement data, good starting values can be obtained to feed the recursive fitting algorithm, ensuring a proper convergence [13]. The $|s_{ij}|$ values obtained using the fitting algorithm across 1520nm-1570 nm is given in

Figure 3(b). The imbalance between $|s_{i1}|$ and $|s_{i2}|$ values could be attributed to the spitting imbalance of the 1×2 MMI splitter.

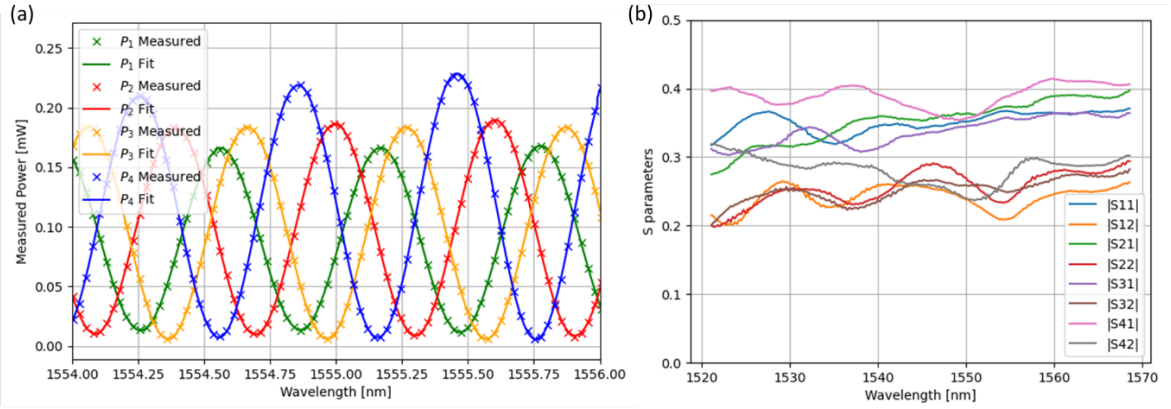

Figure 3 – (a) Measured output powers and the resulting fit functions and (b) obtained values for s-parameter magnitudes

The common mode rejection ratio (CMRR) is a measure for the power imbalance of different output channels when a single input of the MMI is used, and is defined by,

$$CMRR_{jI} = 20\log\left(\frac{|s_{1j}|^2-|s_{4j}|^2}{|s_{1j}|^2+|s_{4j}|^2}\right) \qquad CMRR_{jQ} = 20\log\left(\frac{|s_{2j}|^2-|s_{3j}|^2}{|s_{2j}|^2+|s_{3j}|^2}\right), \qquad (4)$$

where j is the input channel, and the letters I and Q correspond to the output channel pairs for the measurement of in-phase (channels 1 and 4), and quadrature (channels 2 and 3) components. The resulting CMRR values calculated using the obtained s-parameters are shown in the Figure 4(a). All the four CMRR values are below -20dB across 1542-1552 nm.

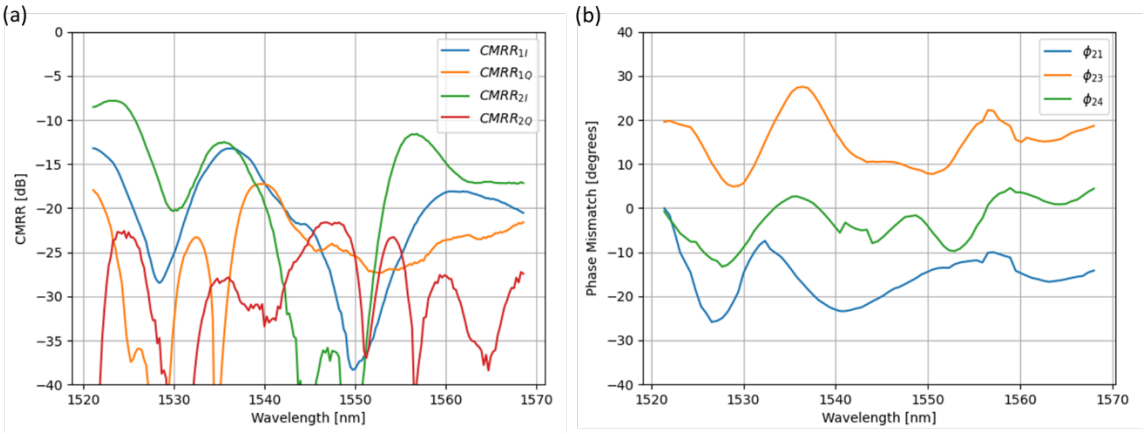

Figure 4 – The calculated (a) CMRR and (b) phase mismatch values

The relative phase offsets of different output channels $\Phi_{ij} = \varphi_i - \varphi_j$ can be calculated from the relative position of the peaks in the transmission spectra of different channels. The phase deviation from an ideal MMI can be found from the difference between the calculated phase offset, and the theoretical phase offset between the output channels, which take the values in $\{\frac{\pi}{2}, \pi, \frac{3\pi}{2}\}$. The calculated phase mismatch values are shown in Figure 4(b). The phase deviation between the output channels are below 15 degrees across

1549nm-1554nm. High phase deviation and low CMRR values are assigned to be due to width and etch depth variations between the designed and the fabricated devices. These will be investigated in more detail and optimized in the next iterations.

Conclusion

The results from an optical 90° hybrid, based on a 4×4 MMI device; together with the method for the extraction of the performance parameters associated with the hybrid is presented. The CMRR values are below -20dB across a wavelength span of 10 nm, and the phase deviation values are below 15 degrees across a wavelength span of 5 nm around a center wavelength of 1550 nm.

Acknowledgements

This work has received funding from the European Union's Horizon 2020 research and innovation programme through the Quantum-Flagship project UNIQORN under grant agreement No 820474. Nazca Design was used to generate the mask layout in this work.

References

[1] S.H. Jeong, and K. Morito, "Novel Optical 90° Hybrid Consisting of a Paired Interference Based 2x4 MMI Coupler, a Phase Shifter and a 2×2 MMI Coupler," Journal of Lightwave Technology 28.9, 1323-1331, 2010.

[2] K. Kikuchi, "Phase-diversity homodyne detection of multilevel optical modulation with digital carrier phase estimation," IEEE Journal of Selected Topics in Quantum Electronics 12.4, 563-570, 2006.

[3] C. R. Doerr, L. Zhang, P. J. Winzer, N. Weimann, V. Houtsma, T-C. Hu, N. J. Sauer et al., "Monolithic InP dual-polarization and dual-quadrature coherent receiver," IEEE Photonics Technology Letters 23.11, 694-696, 2011.

[4] D. Po, X. Liu, S. Chandrasekhar, L. L. Buhl, R. Aroca, and Y.K. Chen, "Monolithic silicon photonic integrated circuits for compact 100 $^{+}$Gb/s coherent optical receivers and transmitters," IEEE Journal of Selected Topics in Quantum Electronics 20.4, 150-157, 2014.

[5] Y. Zhou, J. Sun, A. Yan, Z. Luan, and L. Liu, "Self-homodyne interferometric detection in 2× 4 optical hybrid for free-space optical communication," Free-Space Laser Communications X. Vol. 7814. International Society for Optics and Photonics, 2010.

[6] P.S. Cho, G. Harston, A. Greenblatt, A. Kaplan, Y. Achiam, R. M. Bertenburg, A. Brennemann, B. Adoram, P. Goldgeier, and A. Hershkovit, "Integrated optical coherent balanced receiver," Coherent Optical Technologies and Applications, Optical Society of America, 2006.

[7] D. Hoffman, H. Heidrich, G. Wenke, R. Langenhorst, and E. Dietrich. "Integrated optics eight-port 90 degrees hybrid on $LiNbO_3$," Journal of Lightwave Technology, 7.5, 794-798, 1989.

[8] H. Guan, Y. Ma, R. Shi, X. Zhu, R. Younce, Y. Chen, J. Roman et al., "Compact and low loss 90° optical hybrid on a silicon-on-insulator platform," Optics Express 25.23, 28957-28968, 2017.

[9] W. Yang, M. Yin, Y. Li, X. Wang, and Z. Wang. "Ultra-compact optical 90° hybrid based on a wedge-shaped 2× 4 MMI coupler and a 2× 2 MMI coupler in silicon-on-insulator," Optics Express, 21.23, 28423-28431, 2013.

[10] C. R. Doerr, P.J. Winzer, Y.K.Chen, S. Chandrasekhar, M. S. Rasras, L. Chen, T.Y. Liow, K.W. Ang, and G.Q. Lo, "Monolithic polarization and phase diversity coherent receiver in silicon," Journal of Lightwave Technology, 28.4, 520-525, 2009.

[11] C. R. Doerr, L. Zhang, and P. J. Winzer, "Monolithic InP multiwavelength coherent receiver using a chirped arrayed waveguide grating," Journal of Lightwave Technology 29.4, 536-541, 2011.

[12] S. Farwell, P. Aivaliotis, Y. Qian, P. Bromley, R. Griggs, J.N.Y. Hoe, C. Smith, and S. Jones, "InP coherent receiver chip with high performance and manufacturability for CFP2 modules," OFC 2014.

[13] E. Kleijn, E.M. Van Vliet, D. Pustakhod, M. K. Smit, and X.J.M. Leijtens, "Amplitude and Phase Error Correction Algorithm for 3×3 MMI Based Mach–Zehnder Interferometers," Journal of Lightwave Technology, 33.11, 2233-2239, 2015.